Original Article

Reconfigurable Generation of PAM-4 Signal Based on Fano Effect for Optical Interconnect Systems

Do The Duong[1], Le Duy Tien[2], Nguyen Thi Hong Loan[3],
Hoang Thanh Nhat[2], Le Trung Thanh[2,*]

[1]*University of Transport and Communications (UTC), 3 Cau Giay, Dong Da, Hanoi, Vietnam*
[2]*International School (VNU-IS), Vietnam National University, 144 Xuan Thuy, Cau Giay, Hanoi, Vietnam*
[3]*Hanoi University of Natural Resources and Environment, 41A Phu Dien, Tu Liem, Hanoi, Vietnam*

Abstract: We present a novel low-power architecture for the generation of multilevel pulse amplitude modulation (PAM-4) signal generation. A new structure of a micro-ring resonator based on a 4×4 MMI (Multimode interference) coupler is proposed to control the coupling coefficient and Fano shapes. Based on this structure, a high linearity of the transmission is created, compared with the Mach Zehnder Interferometer (MZI) conventional structure. Here, instead of using directional couplers and MZI as shown in the previous reports, in our method only two 4×4 multimode interference structures on silicon on insulator (SOI) waveguides has been used. The new design is compatible and suitable for the current CMOS fabrication technology. In this work, the special design is as follows: one of two MMI couplers is used to be a micro-ring resonator and two segmented phase shifters are used in the micro-ring resonator to generate 4 levels of the PAM-4 signal. The micro-ring resonator is controlled to work at the over-coupled region, so the Fano effect can be generated. This proposed PAM-4 architecture uses the generated Fano effect, therefore an extreme reduction in power consumption can be achieved. A large fabrication tolerance of ±500 nm and a compact footprint of 10×500 μm^2 can be carried-out. The device is simulated and optimally designed using the FDTD (finite difference time domain) and EME (Eigenmode Expansion). This architecture can be useful for optical interconnects and data center network applications.

Keywords: Optical waveguides, Optical communication equipment, Optical interconnections.

_____

* Corresponding author.
  E-mail address: thanh.le@vnu.edu.vn

1. Introduction

In optical interconnect systems and data center networks, on/off keying (OOK) modulation is used to be employed for the transmitter and receiver topologies. Recently, high speed OOK modulation-based configurations for 200 Gb/s and 400 Gb/s systems have been deployed [1]. However, if a high bandwidth is required, the OOK modulation is constrained and the system becomes much more complex. To avoid this complexity, a new effective higher order modulation is needed. PAM-4 generation is a good candidate for both appropriate cost and low complexity [2]. PAM-4 only needs a little amount of digital signal processing (DSP) resources in comparison to other higher modulations like M-PSK and M-QAM. Although a good signal-to-noise ratio is needed, the PAM-4 modulation enables direct steering of optical intensity signals without any need for complicated DSP. As a result, for data centers and high speed computing systems, PAM-4 has been employed in place of conventional modulation techniques [3].

There are significant works for PAM-4 generation based mainly on micro-ring resonator or MZI configurations. For example, PAM-4 generation are based on silicon photonic micro-ring modulators (MRMs), travelling-wave Mach-Zehnder modulators (TWMZMs) [4], segmented electrode MZI [5], vertical-cavity surface-emitting lasers (VCSEL), silicon-germanium electro-optic modulators, silicon hybrid modulators, electro-optic polymer modulators and LiNbO3 modulators [4]. These approaches require complex circuits, high power and low fabrication tolerance. Power consumption is a critical parameter for applications in optical computing and optical interconnect systems. A new method for PAM-4 generation based on electromagnetically induced transparency (EIT) was proposed for the first time to reduce power consumption [6]. However, this method is not suitable for photonic integrated circuits.

Therefore, in this work, we propose a new architecture to generate a PAM-4 signal with low power consumption and high fabrication tolerance. We present a new method for power reduction by the Fano effect used for PAM-4 generation. In addition, we use only multimode interference structures to create the whole device without a conventional micro-ring resonator and MZI as shown in the literature. We show that a significant reduction in power consumption of 3 to 30 times can be achieved, compared with the conventional MZI architecture. We also design the device using the SOI waveguide. From the simulation results, we show that a large fabrication tolerance of ±500 nm can be achieved. The SOI waveguide can be fabricated by the CMOS existing technologies so it is compatible with CMOS processes [7]. Optical interconnects are the major commercial application of silicon photonics [8]. They are driven by the quickly increasing demand for high-speed optical links in data centers.

2. Generation of PAM-4 Signal Based on Cascaded 4×4 MMIs with Fano Effect

Figure 1a shows a schematic of the PAM-4 generation architecture. Two 4×4 MMI couplers are used to implement the desired PAM-4 generation. We shall show that this structure can create a sharp Fano resonance and both functions acting as an MZI and ring resonator is obtained. We shall control the second MMI coupler that acts as a micro-ring resonator for over-coupled resonance to achieve the Fano effect by using the phase shifters. The phase shifters are shown in white color in the figure [9]. Figure 1b shows the silicon-on-insulator (SOI) rib waveguide structure using the p-n junction to generate the phase shifts.

In our work, we use a micro-ring resonator with a radius of 5 μm and an operating wavelength is 1,550 nm. The waveguide has a width of 500 nm and a height of 220 nm, and it is on a 90-nm slab for a single-mode operation [10]. For PAM-4, we use two bits to generate 4 levels of the PAM-4. In this design, two phase shifters based on the plasma dispersion effect in silicon waveguides are used as shown

in the box of Fig. 1a. The mode profile of the optical waveguide is shown in Fig. 1c, where the effective refractive index is n_{eff}=1.61 by using the FDM (finite difference method).

By using the electrical simulations, we find out the refractive index changes of the waveguide for different applied voltages. Fig. 2 shows plots of the effective index changes and the propagation losses when applying reverse bias voltages on the four p-n junction designs in Fig. 1.

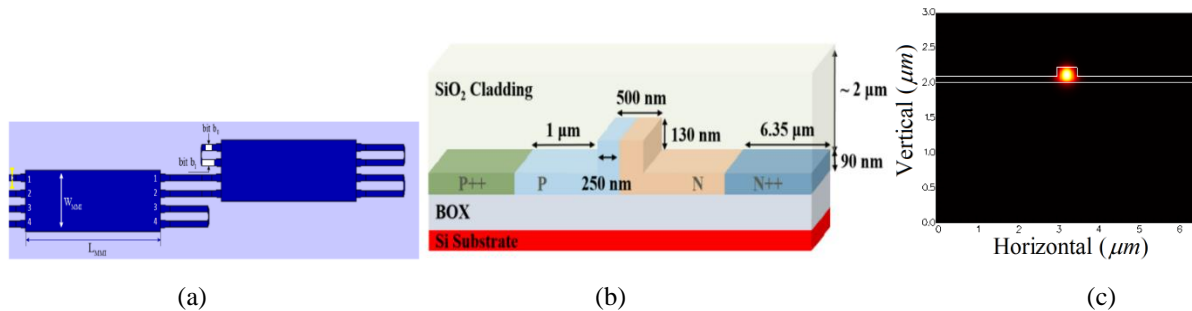| (a) | (b) | (c) |

Figure 1. (a) Scheme of a PAM-4 signaling based on two MMI couplers, (b) cross-sectional view of the phase shifters and (c) fundamental mode of the single mode waveguide.

From these simulation results, one can achieve the phase shifts respecting to bits b_0 and b_1 of the four levels of PAM-4. For PAM-4, the length of phase shifter L_1 for bit b_0 and $L_2 = 2L_1$ for bit b_1 were used with applied voltage V_1 and V_2, respectively. Here, the phase shifter with the length L_1 is for LSB (Least Significant Bit) and L_2 is for MSB (Maximum Significant Bit) of input data bits $b_0 b_1$. The effective index changes were achieved by the plasma dispersion effect in SOI waveguide due to the applied voltages.

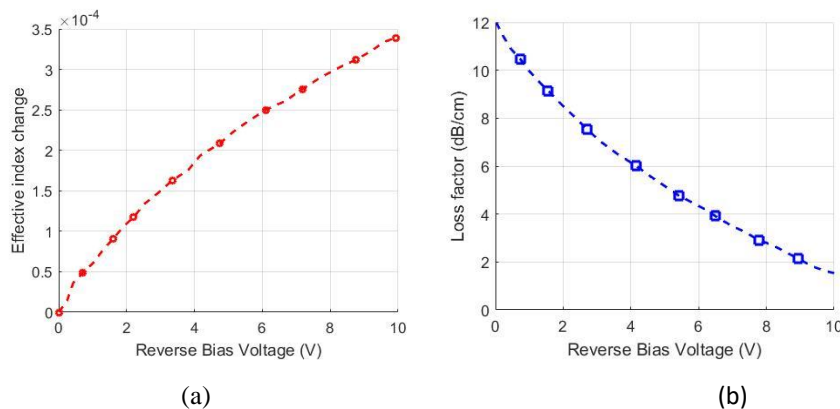| (a) | (b) |

Figure 2. Effective index change (a) and loss factor at different bias voltage at the p-n junction (b).

The key elements of the proposed structures are 4×4 MMI couplers. We need to carefully design the 4×4 MMI coupler to achieve the desired characteristics. We use two steps to design the MMI coupler [11, 12]. Firstly, we use the mode propagation method (MPM) [11] to roughly find out the locations of the input and output waveguides at $x_i = (i + \frac{1}{2}) \frac{W_{MMI}}{N}$ (i=0, 1, 2, 3) as shown in Fig. 1a. Then the 4×4 MMI coupler is optimally designed by the numerical simulations based on 3D-EME (Eigenmode Expansion). As a result, the optimal width of 6 μm and length of 225 μm are achieved, respectively as shown in

Fig. 3a. For the first 4×4 MMI coupler, we use only input port 1 for the input signal of the device and input port 4 for the output signal of the device. By using the 3D-EME, the normalized output powers at output ports 1 and 4 are shown in Fig. 3a.
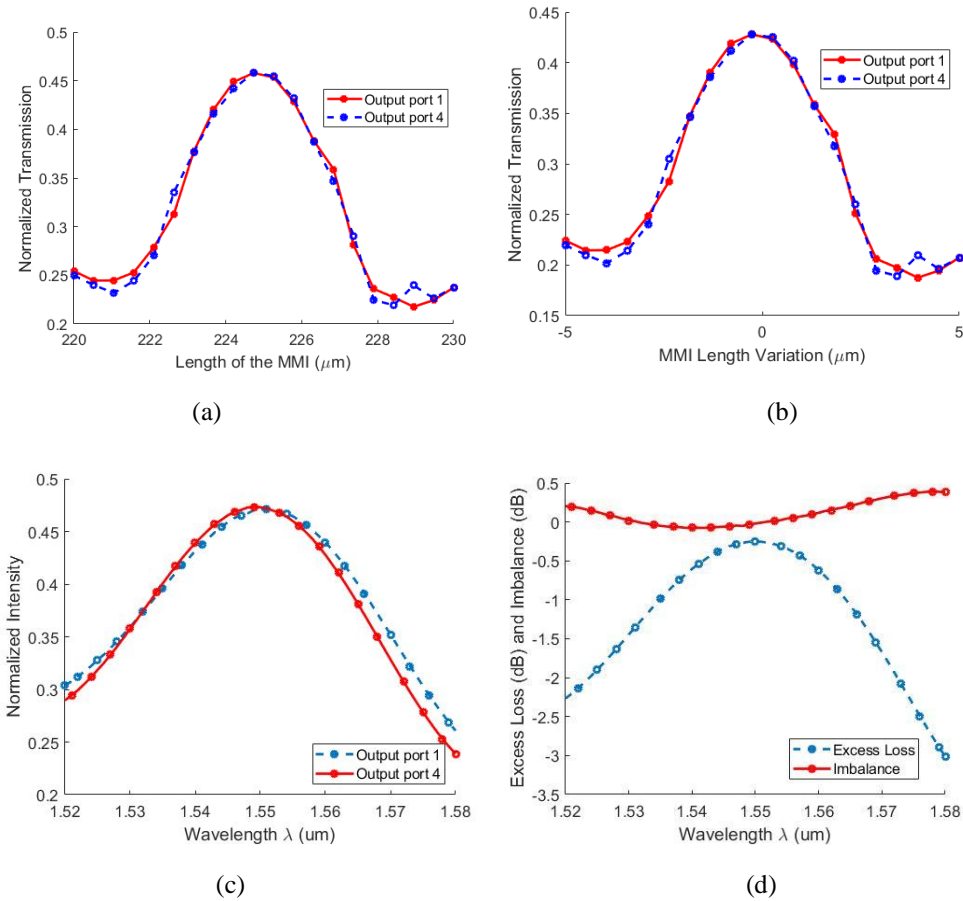

Figure 3. (a) Normalized powers at output ports 1 and 4 at around the optimal width and length of the 4×4 MMI coupler and (b) fabrication tolerance analysis, (c) Bandwidth analysis and (d) loss and imbalance analysis.

Fig. 3b presents the normalized power variations at around the optimal length of 225 µm. From these simulation results, one can see that a fabrication tolerance of ±500 nm can be achieved for a variation in the normalized output powers of 0.02. This variation provides a large fabrication tolerance for the existing CMOS technology [13]. It is reliable for silicon photonics with a minimum fabrication error of ±5 nm [14]. For the fabrication process, silicon photonics foundries typically employ commercially available 193 nm or 248 nm lithography [15]. In general, three different types of fabrication services such as multi-project wafer (MPW) service, customized service and volume production are often used for device fabrication. In practice, MPW is the service that many designers can share the same mask and fabrication process. Thus, the fabrication cost is also shared among designers. Fig. 3c shows the output signals at ports 1 and 4 at different wavelengths. The -1dB bandwidth is about 30 nm from the simulation result in Fig. 3c. The excess loss describes the relation between the input and output powers of the MMI couplers. The excess loss and the imbalance of a 4×4 MMI coupler can be expressed as follows:

$$EL(\ dB\ ) = -10log(\ P_1 + P_4\ ) \tag{1}$$

$$IMB(\ dB\ ) = -10log(\ P_1 / P_4\ ) \tag{2}$$

where P_1 and P_4 are the normalized powers at output ports 1 and 4 of the 4×4 MMI. The excess loss and the imbalance are analyzed in Fig. 3c and Fig. 3d. The simulation results show that bandwidth of 28 nm and 60 nm can be achieved for -1dB excess loss and imbalance, respectively.

For theoretical analysis, the 4×4 MMI coupler is described by a transfer matrix. The phase ϕ_{ij} associated with imaging an input i to an output j in a 4×4 MMI coupler. These phases ϕ_{ij} form a matrix $S_{4\times4MMI}$, with i representing the row number, and j representing the column number. A single 4×4 MMI coupler at a length of $L_{MMI} = \dfrac{3L_\pi}{2}$, where L_π is the beat length of the MMI, is described by the following transfer matrix [16].

$$S_{4x4MMI} = \frac{1}{2} \begin{bmatrix} 1-j & 0 & 0 & 1+j \\ 0 & 1-j & 1+j & 0 \\ 0 & 1+j & 1-j & 0 \\ 1+j & 0 & 0 & 1-j \end{bmatrix} \tag{3}$$

The output and input amplitudes at 4 ports of the 4×4 multimode waveguide can be expressed by

$$\overrightarrow{E_{out}} = \begin{pmatrix} E_{out,1} \\ E_{out,2} \\ E_{out,3} \\ E_{out,4} \end{pmatrix} = \mathbf{S}_{4x4} \begin{pmatrix} E_{in,1} \\ E_{in,2} \\ E_{in,3} \\ E_{in,4} \end{pmatrix} = \mathbf{S}_{4x4} \overrightarrow{E_{in}} \tag{4}$$

Where $E_{in,i}$ (i=1, 2, 3, 4) and $E_{out,j}$ (j=1, 2, 3, 4) are complex amplitudes at input ports and output ports 1-4, respectively.

For the proposed structure in Fig. 1a, the second 4×4 MMI with feedback waveguides at the output ports is used as a micro-ring resonator. In this structure, we use the phase shifter to control the critical coupling of the micro-ring resonator [17].

From equations (3) and (4), we can calculate the relations between the input and output amplitudes of Fig. 1 as follows [18]:

$$\begin{pmatrix} E_{in,1} \\ E_{in,4} \end{pmatrix} = \mathbf{M} \begin{pmatrix} E_{in,2} \\ E_{in,3} \end{pmatrix} = e^{j\frac{\Delta\varphi}{2}} \begin{bmatrix} \tau & \kappa \\ \kappa^* & -\tau^* \end{bmatrix} \begin{pmatrix} E_{in,2} \\ E_{in,3} \end{pmatrix} \tag{5}$$

where $\tau = \cos(\dfrac{\Delta\varphi}{2})$, and $\kappa = \sin(\dfrac{\Delta\varphi}{2})$ are coupling ratios of the micro-ring resonator. The phase shift $\Delta\varphi$ is induced by the p-n junction, can be calculated by:

$$\Delta\varphi = \frac{2L_{PS}}{\lambda} \Delta n_{eff} (V) \tag{6}$$

Where L_{PS} is the length of the phase shifter (p-n junction). As a result, the coupling ratios of the micro-ring resonator based on 4×4 MMI coupler in Fig. 1a can be controlled by the phase shifter as shown in Fig. 4.
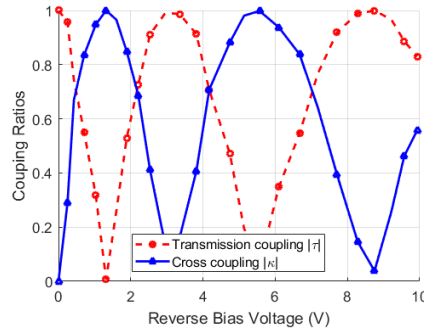
Figure 4. Control of the micro-ring resonator coupling ratio based on the p-n phase shifter.

For a single micro-ring resonator, the fields at output of the micro-ring resonator is expressed by using the Yariv's model [19]:

$$\begin{pmatrix} E_{t1} \\ E_{t2} \end{pmatrix} = \begin{pmatrix} \tau & \kappa \\ -\kappa^* & \tau \end{pmatrix} \begin{pmatrix} E_{i1} \\ E_{i2} \end{pmatrix} \tag{7}$$

where κ and τ are the cross coupling and transmission coupling coefficients of the coupler; $E_{i2} = \alpha \exp(j\phi)E_{t2}$, α is the loss factor of the field after one round trip through the micro-ring resonator; n_{eff} is the effective index and L_R is length of the micro-ring resonator waveguide, R is the radius of the micro-ring waveguide.

The output field and input field of a single micro-ring resonator is:

$$E_{t1} = E_{i1} \frac{-\alpha + \tau e^{-j\phi}}{-\alpha\tau^* + e^{-j\phi}} \tag{8}$$

In Fig. 1a, by applying two electrical signals with applied voltages V_1 and V_2, four distinct levels for data bits 00, 01, 10, 11 are obtained in the output power. Modeling can be used to find out the voltages required to reach 4 equally spaced power levels of PAM-4. The amplitude of the output port is expressed by:

$$E_{out} = \frac{1}{2} E_{in} \left(\frac{-\alpha + \tau e^{-j\phi}}{-\alpha\tau^* + e^{-j\phi}} + e^{-j\theta} \right) \tag{9}$$

where θ is the phase shift at the arm connected between output ports 3 and 4; ϕ is the phase shift inside the micro-ring resonator, including the phase shift due to optical waveguide $\varphi_0 = 4\pi^2 n_{eff} \frac{R}{\lambda}$ and phase shift due to the segmented phase shifters for PAM-4 generation. $\Delta\phi$ is the total phase difference induced by the two phase shift segments L1 and L2.

$$\Delta\phi = \frac{2L_1}{\lambda} \Delta n_{eff}(V_0) + \frac{2L_2}{\lambda} \Delta n_{eff}(V_1) + 4\pi^2 n_{eff} \frac{R}{\lambda} \tag{10}$$

To accumulate the phase shift of single micro-ring resonator into the overall transmission of the device, we carefully design the micro-ring resonator working at the over-coupled condition. The second 4×4 MMI is used for this purpose. The transmissions of the device and phase response of the micro-ring resonator based on the second 4×4 MMI are shown in Fig. 5a and 5b, respectively. From this simulation,

the Fano effect can be achieved if the over-coupled condition of the micro-ring resonator based on the second 4×4 MMI is met.
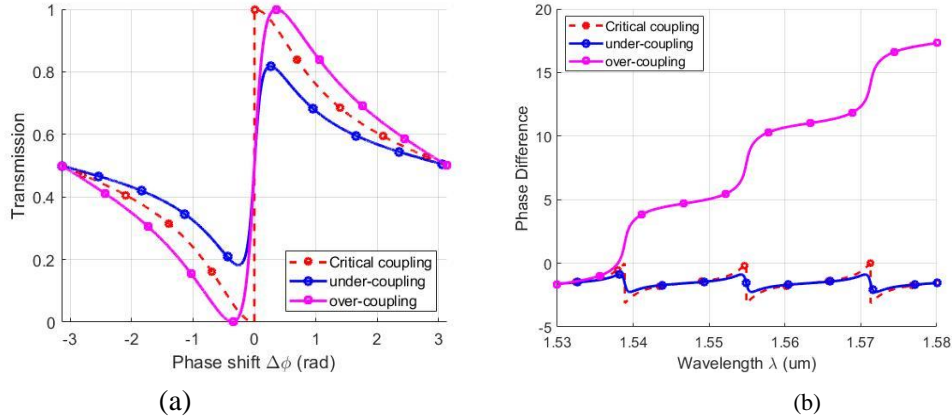

(a)　　　　　　　　　　　　　　　　　　　　　　　　　(b)

Figure 5. (a) Transmissions and (b) phase shift for different cases of the single micro-ring resonator working at critical coupling, under-coupling and over-coupling condition.

In order to control the micro-ring resonator working in the over-coupled region, the loss and coupling ratios is to be investigated. Fig. 6 shows the simulations of the normalized transmissions at different waveguide loss factor inside the micro-ring resonator. The effect of the coupling ratio on the transmission of the device is simulated in Fig. 7. We can see that the coupling ratio has a great effect on the working principle of the PAM-4 generation based on the Fano effect. It is because we need to control the micro-ring resonator to work in the over-coupled region to obtain the Fano effect. By controlling the coupling coefficient ratio, we can achieve a small power to obtain the desired levels of PAM-4.
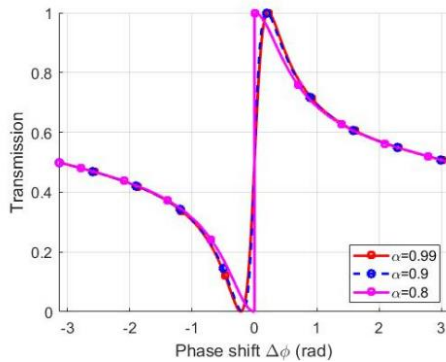

Figure 6. Transmissions at different loss factor for an over-coupled condition.
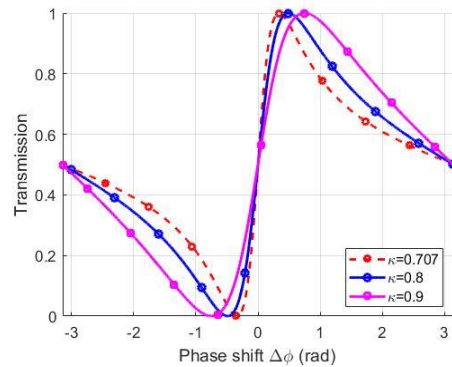
Figure 7. Transmissions at different coupling ratios

Fig. 8 shows the normalized transmissions of the device for different phase shifts and wavelengths. Here for an operating wavelength of 1550 nm, we choose $\theta = \pi/2$ to obtain the Fano effect. We shall show that based on this Fano effect, the proposed structure can reduce required power significantly compared with the structure based on the MZI or MZM configuration. The reduction in the phase shift required for PAM-4 levels translates into a reduction in the required applied power or electrical power. For phase shift calculation, the relation between the required power and the phase shift can be expressed by:

$$\Delta\varphi_i = \frac{\pi}{\Delta P_\pi} P_i \tag{11}$$

where, $\Delta\varphi_i$, P_i (i=0, 1, 2, 3) are the required phase shifts and powers for PAM-4 levels 00, 01, 10, 11 and ΔP_π is the power required to induce phase shift of π (in radian), thus this is equivalent to the switching power for a conventional MZM.

When applying reverse bias voltages, the wavelength is shifted due to the effective index change. The factor VπL (V.cm), which is the required voltage to achieve a π phase shift for a given length L, is typically used. It is calculated as:

$$V_\pi L = \frac{\pi V_{bias} L}{\Delta\varphi} \tag{12}$$

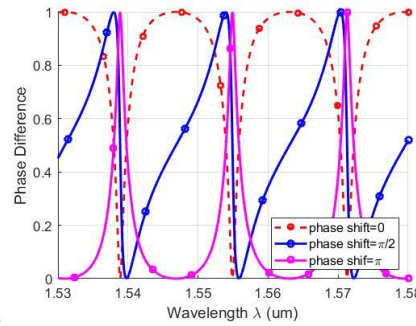where V_{bias} is the applied bias voltage.

Figure 8. Transmissions at different phase shifts.

There are two main methods for PAM-4 signal generation: one is based on the MZM/MZI configuration and the other is based on the micro-ring resonator. For example, the structures such as single drive (SD-MZM) [20], dual drive (DD-MZM) [21], segmented/multi-segmented drive (DD-MIM) [22], push-pull MZM configurations [23] and micro-ring resonator based PAM-4 [24] are reported. Depending on the practical applications, the trade-off between some key parameters of the configurations is required. The extinction ratio (ER) can be increased further by increasing length L or peak-to-peak applied voltage V_{pp} or increasing the linearity of the structure. Here we can select the PAM-4 levels from 0.2 to 0.8 (ER=13.8dB).
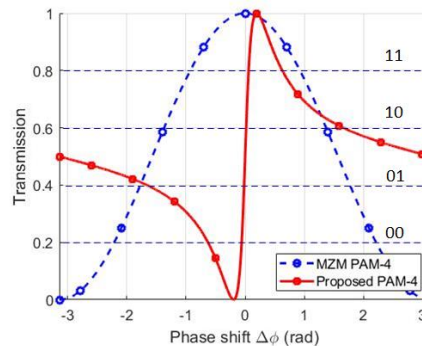

Figure 9. Comparison of the MZM and the proposed PAM-4 generation architecture in this paper.

3. Results and Discussion

The working principle of the PAM-4 signal generation based on the our new structure is shown in Fig. 9. In order to compare the power consumption with the conventional MZI structure, we compare the results based on Fano effect presented in this research with the conventional Mach-Zehnder Modulator (MZM). This result shows that the power consumption to achieve multilevel PAM-4 is extremely low compared with the MZM based PAM-4 generation, but it provides a large fabrication tolerance compared with a conventional structure based on the MZM in the literature. The simulation results are shown for data bits 00, 01, 11, 10, the total phase difference between two arms of Fig. 1a must be -0.06π, -0.02π, 0.02π and 0.06π (rad), respectively. To achieve a linear region, four normalized output powers at 0.2, 0.4, 0.6 and 0.8 are selected. From Fig. 9 and Eq. (9), the phase shift is reduced from 3 times to 30 times at different PAM-4 levels respectively, compared with the phase shift required when the MZM/MZI is used.

At the final design step, we use FDTD simulation to verify the whole working principle of the proposed device. Two MMI couplers with phase shifters are shown in Fig. 10 in the FDTD environment. In order to generate the PAM-4, we use the phase shifters of -0.06π, -0.02π, 0.02π and 0.06π(rad) injected into the segmented phase shifters of Fig. 1a, respectively. Figure 10 shows the field propagation over the whole structure. The normalized output powers for 4 PAM-4 levels are calculated to be approximately 0.2, 0.4, 0.6 and 0.8. It is noted that, our design can provide the input and output signals are at the same side. This characteristic can be suitable for photonic integrated circuits for optical interconnect systems. For the numerical simulations, we use a Gaussian light pulse of 15 fs pulse width. The grid sizes $\Delta x=\Delta y=5$ nm and $\Delta z=10$ nm are chosen.

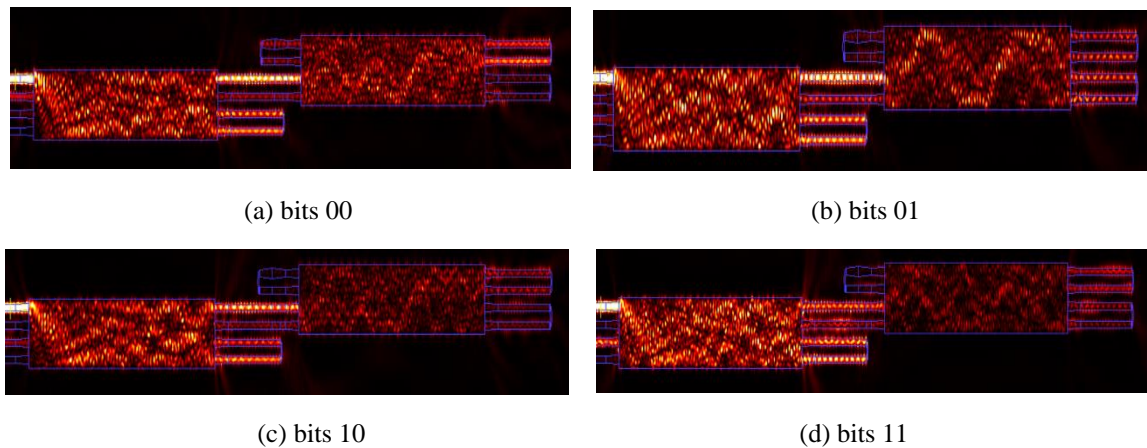|	
(a) bits 00	(b) bits 01
(c) bits 10	(d) bits 11

Figure 10. FDTD simulation of the whole device when input signal
is at port 1 for 4 cases of data bits 00, 01, 10, 11.

4. Conclusion

We have presented a new approach for PAM-4 signal generation implementation based on the Fano effect generated from two 4×4 MMI couplers with feedback waveguide. The proposed configuration can provide a good fabrication tolerance of ±500 nm and a power reduction of 3 to 30 times compared with the PAM-4 generation structures based on the MZI/MZM. The proposed structure may be

particularly suitable for complex systems with some channels integrated on a chip. The proposed approach is also suitable and useful for high-performance computing, multicore and high speed data center systems.

Acknowledgments

References

[1] C. Xie et al., 400-Gb/s PDM-4PAM WDM System Using a Monolithic 2×4 VCSEL Array and Coherent Detection, Journal of Lightwave Technology, Vol. 33, No. 3, 2015, pp. 670-677, https//doi.org/10.1109/JLT.2014.2363017.

[2] K. Wang, M. Kong, W. Zhou, J. Ding, J. Yu, 200-Gbit/s PAM4 Generation by a Dual-Polarization Mach-Zehnder Modulator Without DAC, IEEE Photonics Technology Letters, Vol. 32, No. 18, 2020, pp. 1223-1226, https//doi.org/10.1109/LPT.2020.3017535.

[3] L. N. Binh, Optical Modulation: Advanced Techniques and Applications in Transmission Systems and Networks CRC Press, 2019.

[4] W. Shi, Y. Xu, H. Sepehrian, S. LaRochelle, L. A. Rusch, Silicon Photonic Modulators for PAM Transmissions, Journal of Optics, Vol. 20, No. 8, 2018, pp. 083002, https//doi.org/10.1088/2040-8986/aacd65.

[5] M. Kim, D. H. Kwon, D. W. Rho, W. Y. Choi, A Low-Power 28-Gb/s PAM-4MZM Driver with Level Pre-Distortion, IEEE Transactions on Circuits and Systems II: Express Briefs, Vol. 68, No. 3, 2021, pp. 908-912, https//doi.org/10.1109/TCSII.2020.3020128.

[6] J. Wang et al., Optical PAM-4 Generation Via Electromagnetically Induced Transparency in Nitrogen-vacancy Centers, Results in Physics, Vol. 30, 2021, pp. 104802, https://doi.org/10.1016/j.rinp.2021.104802.

[7] X. Wang et al., High-speed silicon Photonic Mach–Zehnder Modulator at 2 μm, Photon. Res., Vol. 9, No. 4, 2021, pp. 535-540, https//doi.org/10.1364/PRJ.417107.

[8] R. Pitwon et al., Evolution of System Embedded Optical Interconnect in Sub-Top-of-Rack Data Center Systems, Applied Sciences, Vol. 12, No. 3, 2022, https//doi.org/ 10.3390/app12031565.

[9] R. D. Demers, S. L. Rochelle, W. Shi, Low-power DAC-less PAM-4 Transmitter using A Cascaded Microring Modulator, Optics Letters, Vol. 41, No. 22, 2016, pp. 5369-5372, https//doi.org/10.1364/ol.41.005369.

[10] R. Li et al., High-speed Low-chirp PAM-4 transmission Based on Push-pull Silicon Photonic Microring Modulators, Optics Express, Vol. 25, No. 12, 2017, pp. 13222-13229, https//doi.org/10.1364/oe.25.013222.

[11] T. T. Le, L. Cahill, Generation of Two Fano Resonances using 4x4 Multimode Interference Structures on Silicon Waveguides, Optics Communications, Vol. 301-302, 2013, pp. 100-105.

[12] J. M. Heaton, R. M. Jenkins, General Matrix Theory of Self-imaging in Multimode Interference(MMI) Couplers, IEEE Photonics Technology Letters, Vol. 11, No. 2, 1999, pp. 212-214.

[13] Y. Hao et al., Recent Progress of Integrated Circuits and Optoelectronic Chips, Science China Information Sciences, Vol. 64, No. 10, 2021, pp. 201401, https//doi.org/10.1007/s11432-021-3235-7.

[14] M. J. Deen, P. K. Basu, Silicon Photonics: Fundamentals and Devices, Wiley Series in Materials for Electronic & Optoelectronic Applications, 2012.

[15] S. Y. Siew et al., Review of Silicon Photonics Technology and Platform Development, Journal of Lightwave Technology, Vol. 39, No. 13, 2021, pp. 4374-4389, https//doi.org/10.1109/JLT.2021.3066203.

[16] T. T. Le, L. Cahill, The Design of 4×4 Multimode Interference Coupler Based Microring Resonators on an SOI Platform, Journal of Telecommunications and Information Technology, Poland, 2009, pp. 98-102.

[17] A. Yariv, Critical Coupling and Its Control in Optical Waveguide-Ring Resonator Systems, IEEE Photonics Technology Letters, Vol. 14, 2002, pp. 483-485.

[18] T. T. Le, D. T. Le, High FSR and Critical Coupling Control of Microring Resonator Based on Graphene-Silicon Multimode Waveguides, in Electromagnetic Propagation and Waveguides in Photonics and Microwave Engineering, P. Steglich Ed: IntechOpen, 2020, https//doi.org/10.5772/intechopen.92210.

[19] A. Yariv, Universal Relations for Coupling of Optical Power Between Microresonators and Dielectric Waveguides, Electronics Letters, Vol. 36, 2000, pp. 321-322.

[20] H. Zhang et al., 800 Gbit/s Transmission Over 1 km Single-mode Fiber using A Four-channel Silicon Photonic Transmitter, Photon. Res., Vol. 8, No. 11, 2020, pp. 1776-1782, https//doi.org/10.1364/PRJ.396815.

[21] T. Ferrotti et al., Co-integrated 1.3um Hybrid III-V/silicon Tunable Laser and Silicon Mach-zehnder Modulator Operating at 25Gb/s, Optics Express, Vol. 24, No. 26, 2016, pp. 30379-30401, https//doi.org/10.1364/OE.24.030379.

[22] D. Patel et al., Design, Analysis, and Transmission System Performance of a 41 GHz Silicon Photonic Modulator, Optics Express, Vol. 23, No. 11, 2015, pp. 14263-14287, https//doi.org/10.1364/OE.23.014263.

[23] R. Ding et al., High-Speed Silicon Modulator with Slow-Wave Electrodes and Fully Independent Differential Drive, Journal of Lightwave Technology, Vol. 32, No. 12, 2014, pp. 2240-2247, https//doi.org/10.1109/JLT.2014.2323954.

[24] M. S. Hai, M. M. P. Fard, O. L. Ladouceur, A Ring-Based 25 Gb/s DAC-Less PAM-4 Modulator, IEEE Journal of Selected Topics in Quantum Electronics, Vol. 22, No. 6, 2016, pp. 123-130, https//doi.org/10.1109/JSTQE.2016.2584978.